Stability and diffusion of interstitial and substitutional Mn in GaAs of different doping types

L. M. C. Pereira,[1,2,3,*] U. Wahl,[3] S. Decoster,[1] J. G. Correia,[3] L. M. Amorim,[1] M. R. da Silva,[4] J. P. Araújo,[2] and A. Vantomme[1]

[1]*Instituut voor Kern en Stralingsfysica, Katholieke Universiteit Leuven, 3001 Leuven, Belgium*

[2]*Instituto de Física dos Materiais da Universidade do Porto, Institute of Nanoscience and Nanotechnology, Universidade do Porto, 4169-007 Porto, Portugal*

[3]*Instituto Tecnológico e Nuclear, Instituto Superior Técnico, Universidade Técnica de Lisboa, 2686-953 Sacavém, Portugal*

[4]*Centro de Física Nuclear da Universidade de Lisboa, 1649-003 Lisboa, Portugal*

(Received 20 June 2012; revised manuscript received 20 July 2012; published 24 September 2012)

We report on β^- emission channeling experiments on the lattice location and thermal stability of Mn impurities (<0.05%) in both semi-insulating and heavily n-type doped GaAs. In addition to the majority of the Mn impurities substituting for Ga, up to 30% occupy tetrahedral interstitial sites with As nearest neighbors. Whereas the interstitial fraction is stable up to 400 °C, with an activation energy for diffusion of 1.7–2.3 eV, substitutional Mn diffuses only at ∼700 °C with an activation energy of ∼3 eV. By comparing these results to those of recent emission channeling experiments on heavily p-type doped GaAs [L. M. C. Pereira *et al.*, Appl. Phys. Lett. **98**, 201905 (2011)], we conclude that the observed high thermal stability of the interstitial fraction cannot be ascribed to trapping by charged defects, but is an intrinsic characteristic of isolated interstitial Mn in the low doping regime (<0.05% Mn). Compared to ferromagnetic $Ga_{1-x}Mn_xAs$ (few percent Mn), for which a significantly lower activation energy has been reported, these findings motivate a comprehensive assessment of how the thermal stability and the diffusion of interstitial Mn are affected by the Mn concentration.

DOI: 10.1103/PhysRevB.86.125206 PACS number(s): 75.50.Pp, 61.72.uj, 61.72.Cc

I. INTRODUCTION

Mn-doped GaAs ($Ga_{1-x}Mn_xAs$) has become the canonical material in which to study the physics of carrier-mediated ferromagnetism in semiconductors[1–4] and the associated phenomena of interest for semiconductor spintronics.[5] Despite being one of the most intensively studied and well-understood dilute magnetic semiconductors, a fundamental question remains unanswered, i.e., *if* and *how* the Curie temperature (T_C) can be increased from the current record values of ∼200 K to above room temperature.[4,6,7]

It has been theoretically and experimentally established that the T_C of $Ga_{1-x}Mn_xAs$ increases with increasing Mn concentration x and hole concentration p.[7] More precisely, T_C increases with effective Mn concentration, which takes into account the balance between the fractions of Mn substituting for Ga (Mn_{Ga}) and on interstitial sites (Mn_I). While Mn_{Ga} provides both the localized magnetic moment and the itinerant hole that mediates the magnetic coupling, Mn_I has a twofold compensating effect: (i) magnetically, as Mn_I-Mn_{Ga} pairs couple antiferromagnetically, and (ii) electrically, since double donor Mn_I compensates Mn_{Ga} acceptors. As a consequence of this self-compensation, while the Mn concentration x that can be incorporated in high-quality $Ga_{1-x}Mn_xAs$ has been increasing throughout the years up to $x \approx 0.20$,[8] p and T_C (of as-grown layers) do not follow.[7] Thermal annealing near the growth temperature (∼200 °C) increases p and consequently T_C, but a significant fraction of the initially introduced Mn atoms remains inactive.[7,9] This partial activation by annealing (∼200 °C) was attributed to the out-diffusion of a compensating defect with low thermal stability,[9] with an activation energy (E_a) of 0.7 eV,[10] consistent with the predicted diffusion behavior of interstitial Mn in highly Mn-doped, ferromagnetic $Ga_{1-x}Mn_xAs$.[10,11]

Recently, we reported on the lattice location and thermal stability of Mn impurities in heavily p-type (Zn) doped GaAs, in the low Mn-doping regime (<0.05%).[12] We identified the lattice site occupied by interstitial Mn as the tetrahedral interstitial site with As nearest neighbors (T_{As}) and, more importantly, gave evidence of its high thermal stability, up to 400 °C, with an effective activation energy for diffusion of 1.7–2.3 eV. Such pronounced decrease in E_a, from the low doping (<0.05% in Ref. 12) to the high doping (few percent in Ref. 10) regimes, challenges our understanding of the diffusion behavior of interstitial Mn in GaAs. On the one hand, such higher E_a in the low doping regime may result from trapping of Mn_I by oppositely charged acceptor defects. Indeed, while the migration barrier for isolated Mn_I was estimated by *ab initio* calculations to be only 0.8 eV,[10] pairing with Mn_{Ga} acceptors was estimated to add up to 0.8 eV of binding energy.[13] On the other hand, it may be a direct consequence of the low Mn concentration. Indeed, the basic electrical and magnetic properties of $Ga_{1-x}Mn_xAs$ are fundamentally different in the low doping regime.[14]

We address this question here by studying, as a function of annealing temperature, the lattice location of Mn in both semi-insulating (s.i.) and highly n-type doped (n^+) GaAs using β^- emission channeling (EC). Comparing these to our previous results on highly p-type doped (p^+) GaAs,[12] we investigate if the high thermal stability of interstitial Mn can be ascribed to trapping by charged defects.

II. EXPERIMENT

A. Emission channeling

The EC technique has been developed to study the lattice location of impurities in single crystals, making use of the charged particles emitted by a radioactive isotope of the impurity element under study.[15] The screened Coulomb potential of atomic rows and planes determines the anisotropic scattering of the particles emitted isotropically during decay.

Along low-index crystal directions of single crystals, this anisotropic scattering results in well-defined channeling or blocking effects. Because these effects strongly depend on the initial position of the emitted particles, they lead to emission patterns which are characteristic of the lattice site(s) occupied by the probe atoms. Angular-dependent emission patterns are recorded along various crystallographic axes using a position- and energy-sensitive detection system similar to that described in Ref. 16. The theoretical emission patterns for probes occupying possible lattice sites are calculated using the *many-beam* formalism for electron channeling in single crystals.[15] Quantitative lattice location is provided by fitting the experimental patterns with theoretical ones using the two-dimensional fit procedure outlined in Ref. 17. Corrections for secondary electrons that reach the detector were implemented by subtracting an isotropic background from every pattern. This secondary electron contribution is estimated based on GEANT4[18,19] simulations of electron scattering, taking into account the elemental composition and geometry of the sample, sample holder, and vacuum chamber. Several reviews on emission channeling can be found in the literature.[15,20–22]

Because EC makes use of two-dimensional emission patterns (measured using position sensitive detectors) which are directly compared to numerical simulations, it provides unambiguous and quantitative lattice location. Probably one of the strongest features of the EC technique is its applicability to those cases where significant fractions of the impurities occupy more than one lattice site. This multisite lattice location capability of EC has allowed us, for example, to establish the amphoteric nature (both Ga- and N-substitutional) of As in GaN[23] and to identify, in addition to the majority fractions in cation sites, significant fractions of Co and Mn impurities in the anion (O) site in ZnO.[24]

Examples for possible lattice sites of high symmetry in the GaAs zinc-blende structure are shown in Fig. 1. In addition to the substitutional Ga (S_{Ga}) and As (S_{As}) sites and the tetrahedral interstitial sites with Ga (T_{Ga}) and As (T_{As}) nearest neighbors, a number of other interstitial sites are shown. Figure 2 shows the theoretical emission patterns along the ⟨100⟩, ⟨111⟩, ⟨110⟩, and ⟨211⟩ axes for 100% of ^{56}Mn atoms on substitutional sites (S_{Ga} and S_{As}) and tetrahedral interstitial sites (T_{Ga} and T_{As}). Since S_{Ga}, S_{As}, T_{Ga}, and T_{As} sites are located on the same row along the ⟨111⟩ axis (Fig. 1), they are all equivalent in the lattice projection onto the plane perpendicular to the ⟨111⟩ direction and, consequently, the corresponding pairs of ⟨111⟩ emission patterns are undistinguishable (Fig. 2, second row). Similarly, along the ⟨100⟩ direction, because S_{Ga} is on the same row as T_{As}, and S_{As} is on the same row as T_{Ga}, the corresponding ⟨100⟩ emission patterns are undistinguishable. In order to distinguish these sites it is thus necessary to measure also along the ⟨110⟩ and ⟨211⟩ directions, which separate the corresponding rows (see the dashed lines in Fig. 1). This results in emission patterns with clearly distinct anisotropies (Fig. 2, third and fourth rows). In particular, due to the mirror asymmetry of the ⟨110⟩ and ⟨211⟩ directions, the two T sites are unambiguously distinguished (patterns inside the gray rectangle in Fig. 2).

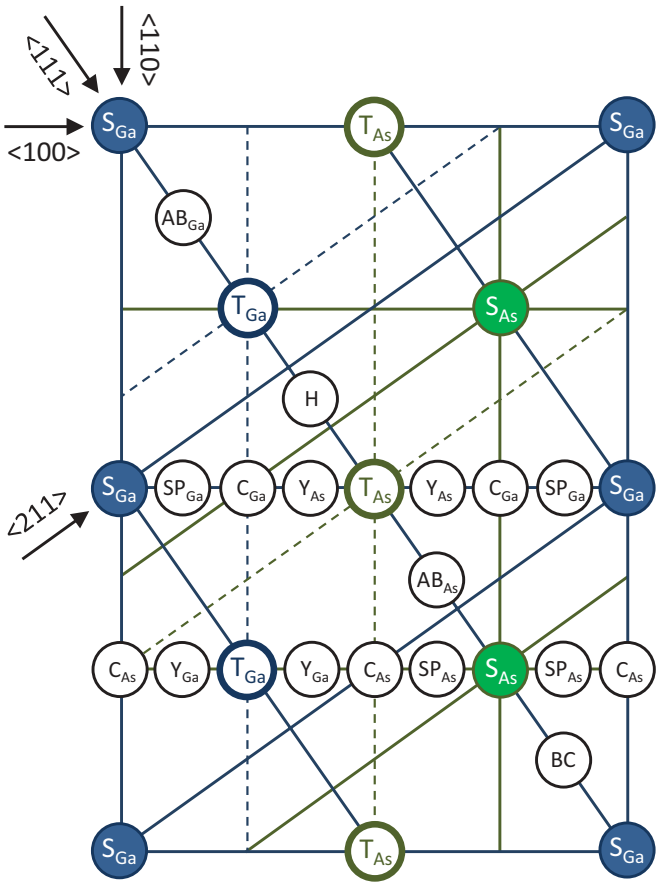

FIG. 1. (Color online) The {110} plane in the GaAs zinc-blende lattice, showing the following sites: the substitutional Ga (S_{Ga}) and As (S_{As}) sites; the tetrahedral interstitial sites with Ga (T_{Ga}) and As (T_{As}) nearest neighbors; interstitial sites along the ⟨111⟩ direction, i.e., the bond center (BC), antibonding Ga (AB_{Ga}), antibonding As (AB_{As}), and the hexagonal site (H); and the interstitial sites along the ⟨100⟩ direction, in either the Ga or the As rows, i.e., the split interstitials (SP_{Ga} and SP_{As}), the "C" sites with C_{2v} symmetry (C_{Ga} and C_{As}), and the "Y" sites (Y_{Ga} and Y_{As}). Along the ⟨100⟩, ⟨111⟩, ⟨110⟩, and ⟨211⟩ directions, the rows of Ga and As atoms are indicated (lines), as are the rows of the T_{Ga} and T_{As} sites (dashed lines). Note that, along the ⟨111⟩ direction, the substitutional (S_{Ga} and S_{As}) and tetrahedral interstitial (T_{Ga} and T_{As}) sites are all located on the same row; along the ⟨100⟩ direction, S_{Ga} is on the same row as T_{As}, and S_{As} is on the same row as T_{Ga}.

B. Experimental details

Radioactive ^{56}Mn ($t_{1/2} = 2.56$ h) was implanted at the on-line isotope separator facility ISOLDE at CERN, which provides mass-separated beams of radioactive Mn isotopes produced by means of 1.4-GeV proton-induced nuclear fission from uranium carbide UC_2 targets and chemically selective laser ion sources.[26] The samples consisted of ⟨100⟩ GaAs single crystals, undoped semi-insulating (s.i.) and heavily n-type doped (n^+). Material properties and implantation details are summarized in Table I, where our previous experiments on heavily p-type doped (p^+) GaAs[12] are also included. All implantations were performed at room temperature under a tilt angle of 17°. Angular-dependent emission yields of the β^-

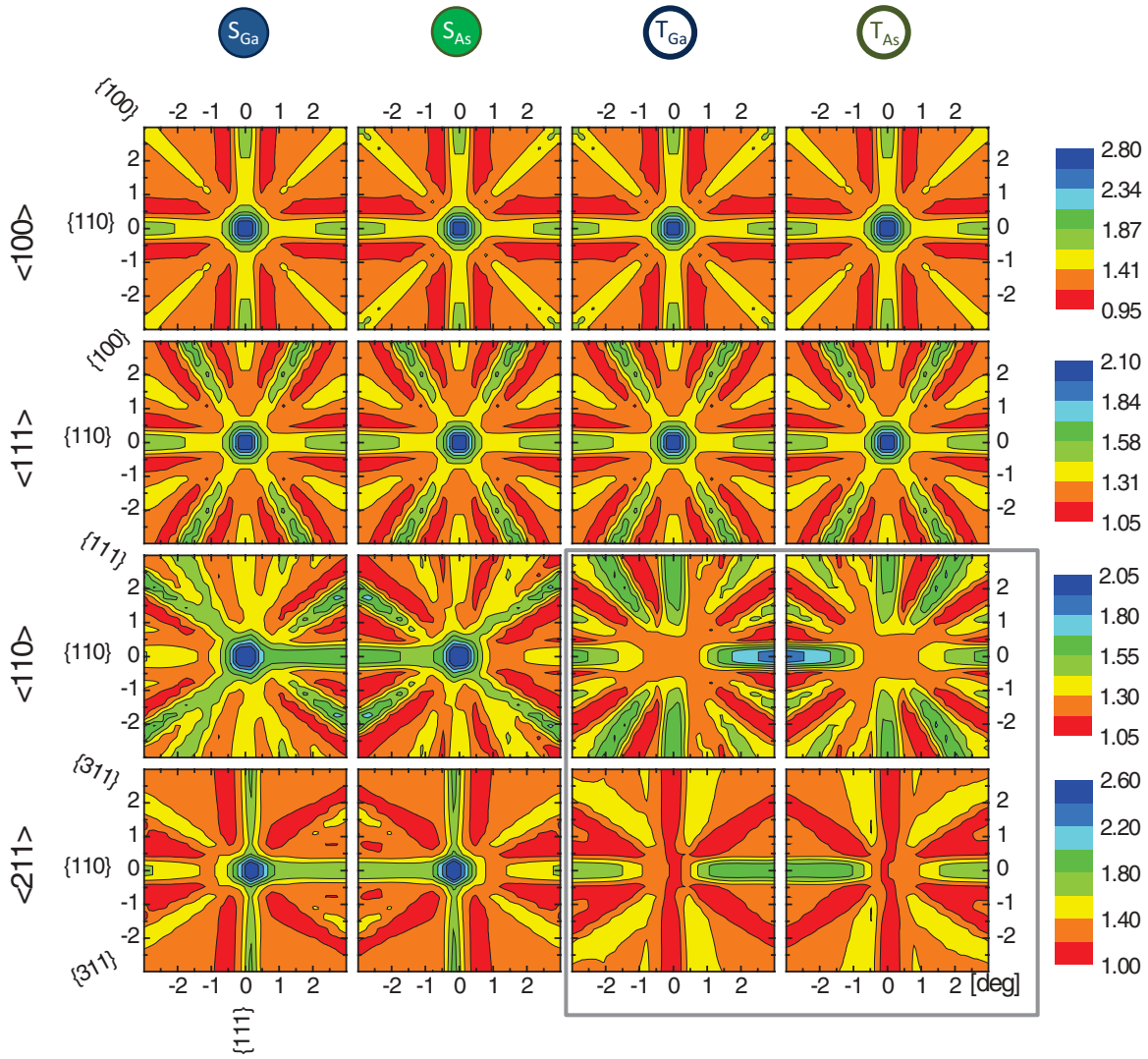

FIG. 2. (Color online) Simulated emission channeling patterns, along the ⟨100⟩, ⟨111⟩, ⟨110⟩, and ⟨211⟩ directions, for 100% of emitter atoms (^{56}Mn) on substitutional Ga (S_{Ga}) and As (S_{As}) sites and tetrahedral interstitial sites with Ga (T_{Ga}) and As (T_{As}) nearest neighbors.

particles emitted during decay to stable ^{56}Fe were measured at room temperature, along four crystallographic directions, ⟨100⟩, ⟨111⟩, ⟨110⟩, and ⟨211⟩, in the as-implanted state and after *in situ* capless annealing in vacuum ($<10^{-5}$ mbar) for 10 min in steps of 100°C from 100 to 700°C. These patterns were recorded using a position- and energy-sensitive detection system similar to that described in Ref. 16. Given the relatively short half-life of ^{56}Mn, this system was installed on-line and upgraded with self-triggering readout chips for the Si pad detectors, enabling measurements during and/or immediately after implantation with count rates of up to several kHz.

Theoretical patterns were calculated for probes occupying substitutional Ga (S_{Ga}) and As (S_{As}) sites with varying root-mean-square (rms) displacements, the high-symmetry interstitial sites described above, and interstitial sites resulting from static displacements along the ⟨100⟩ and ⟨111⟩ directions.

TABLE I. Sample and implantation details. All implantations were performed at room temperature under a tilt angle of 17°. The ^{56}Mn peak concentration (x_p) and the projected ion range (R_p) and straggling were estimated using the SRIM-2008 code.[25] The details of our previous work on p^+ GaAs[12] are also included.

Doping type	Dopant	Resistivity (Ω cm)	Carrier concentration (cm^{-3})	^{56}Mn fluence (at. cm^{-2})	Implantation energy (keV)	Projected ion range (R_p) (Å)	Projected ion straggling (Å)	Peak ^{56}Mn concentration (at. cm^{-3})
n^+	Te	$0.6-2\times10^{-3}$	$1.1-5\times10^{18}(e^-)$	2×10^{13}	40	259	141	5.2×10^{18}
s.i.	–	1.4×10^{8}	–	2×10^{13}	30	206	113	7.2×10^{18}
p^+	Zn	$0.6-2\times10^{-3}$	$1.4-6\times10^{19}(h^+)$	2×10^{13}	50	313	168	4.4×10^{18}

The GaAs crystallographic parameters and room-temperature atomic displacements used in the many-beam simulations can be found in Ref. 27.

III. RESULTS AND DISCUSSION

In the following, we present and discuss the results in two parts. First we determine the lattice sites occupied by Mn in GaAs, in particular with respect to T_{As} versus T_{Ga} interstitial sites. We then analyze the changes observed upon annealing in terms of thermal stability and diffusion.

A. Lattice location: substitutional and *T* interstitial sites

For both n^+ and semi-insulating GaAs, for all four measured directions, the calculated S_{Ga} patterns give by far the best agreement, showing that the majority of the probe atoms occupy Ga sites, as expected. The fitting routine was then allowed to include, in addition to S_{Ga}, a second lattice site, for which all the simulated sites were tested. The $S_{Ga} + T_{As}$ double occupancy gives the best fit compared to all other combinations and considerably improves the S_{Ga} single-site fit (up to 30% improvement in reduced χ^2). As an example for the good match between experiment and simulated patterns, Fig. 3 compares the normalized experimental β^- emission yields along the four directions [(a)–(d)] of the as-implanted n^+ sample with the best fits of theoretical patterns [(e)–(h)]. These fits correspond to a mixed occupancy of 77% on substitutional Ga sites (S_{Ga}) and 20% in tetrahedral interstitial

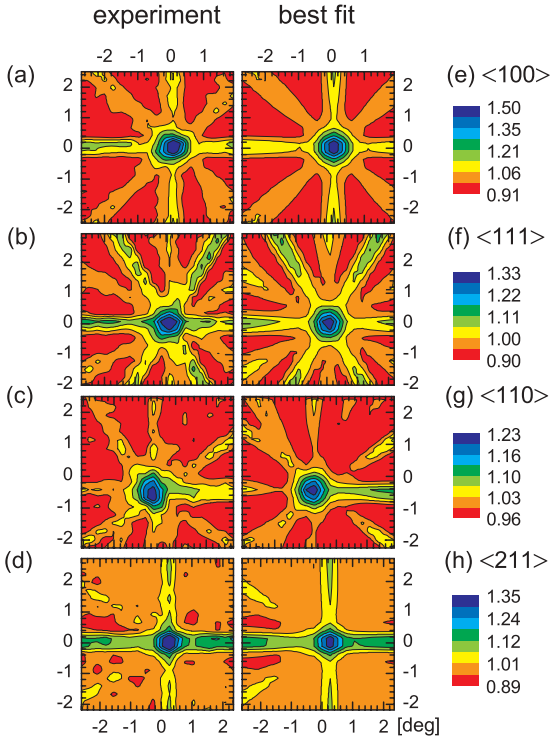

FIG. 3. (Color online) (a)–(d) Normalized experimental β^- emission channeling patterns of the the as-implanted n^+ sample in the vicinity of the ⟨100⟩, ⟨111⟩, ⟨110⟩, and ⟨211⟩ directions. (e)–(h) Corresponding best fits yielding 77 and 20% of the Mn atoms on S_{Ga} and T_{As} sites, respectively.

sites with As nearest neighbors (T_{As}). Introducing a third site yields only insignificant fit improvements (of the order of 1% improvement in reduced χ^2). Possible fractions on other sites are estimated to be below 5%, which is close to the technique's sensitivity limit for detecting small fractions in minority sites. In particular for T_{As} versus T_{Ga} sites, the fitted T_{Ga} fraction is always below 5% (with an improvement in reduced χ^2 of the order of 1%) when the routine is allowed to include S_{Ga}, T_{As}, and T_{Ga} sites simultaneously. This identification of the T_{As} site over T_{Ga} is consistent with our previous results on p^+ GaAs[12] and *ab initio* calculations yielding a 0.35-eV lower energy for Mn in T_{As} sites compared to T_{Ga}.[10] Indeed, due to the Coulomb interaction, positively charged Mn_I^{2+} defects are likely to have a lower energy when coordinated by negatively charged As anions rather than by positively charged Ga cations.

We must note, however, that the T_{As} site may be energetically favorable over T_{Ga} only for *isolated* Mn_I defects. For very high Mn concentrations (a few at. %), the probability of formation of substitutional-interstitial (Mn_{Ga}-Mn_I) pairs or even larger complexes is not negligible. In such complexes, the Coulomb attraction between oppositely charged Mn_{Ga} acceptors and Mn_I donors may counteract the repulsion between positively charged Mn_I and Ga cations: since the distance between neighboring S_{Ga} and T_{Ga} sites (2.45 Å) is smaller than that between neighboring S_{Ga} and T_{As} sites (2.83 Å), the decrease in Coulomb energy by decreasing the Mn_{Ga}-Mn_I distance may counterbalance the increase in Coulomb energy by changing the Mn_I coordination to Ga cations. Indeed, *ab initio* calculations have predicted that the energy of a Mn_I atom in one of the four T_{Ga} sites neighboring a Mn_{Ga} defect is the same as in one of the six T_{As} sites.[10] Moreover, it was also predicted that the energy barrier between the two sites is small enough to allow for Mn_I atoms to swap between the two configurations even at room temperature.[10] Therefore, one can not exclude that, for very high Mn concentrations and when Mn_{Ga}-Mn_I pairs *do* form, part of the interstitial fraction occupies T_{Ga} sites.

B. Thermal stability and diffusion

The Ga-substitutional and T_{As} interstitial fractions are shown in Fig. 4, as a function of annealing temperature, for both n^+ and semi-insulating GaAs. The results of our previous experiments on p^+ GaAs are also included.[12] The behavior is strikingly similar for all three doping types and can be divided in three annealing temperature (T_a) regimes:

(1) $T_a \leqslant 300\,^\circ$C: About 70% of the implanted Mn substitutes for Ga while the remaining 30% occupies T_{As} sites. Within the experimental error, the total $S_{Ga} + T_{As}$ fraction is 100%, which confirms that fractions on other sites are indeed negligible. The increase in the interstitial fraction from ∼20 to ∼30% following annealing at 100 °C is quite reproducible in the three experiments, which indicates that it is not mere scattering of experimental data. An increase in interstitial Mn at the expense of the substitutional fraction can in principle be explained as follows. If the Ga interstitials created during implantation become mobile at temperatures $\leqslant$100 °C, they can migrate during the annealing at 100 °C and either recombine with Ga vacancies or replace substitutional Mn atoms via a kick-out mechanism ($Mn_{Ga} + Ga_I \rightarrow Mn_I +$

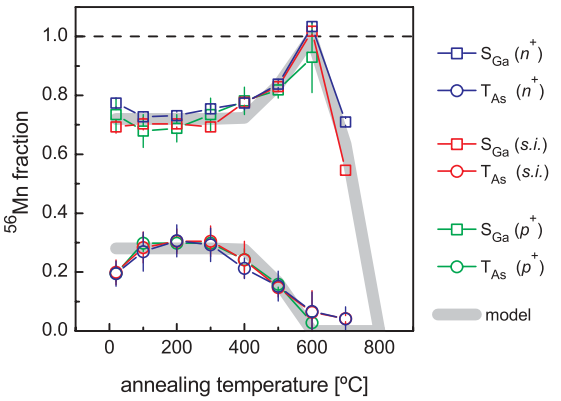

FIG. 4. (Color online) Fractions of ^{56}Mn in S_{Ga} (□) and T_{As} (○) sites in n^+, semi-insulating, and p^+ GaAs, derived from the fits to the experimental patterns. The data for p^+ GaAs are from Ref. 12. The gray line is given by the model of vacancy-limited diffusion of interstitial and substitutional Mn, described in the text.

Ga_{Ga}). The latter mechanism can thus explain the increase of the interstitial fraction at the expense of substitutional Mn. Note that, due to the Coulomb attraction between (most likely) oppositely charged Ga interstitials (donors) and substitutional Mn (acceptors), this kick-out mechanism may be quite efficient even in the very dilute regime of our samples.

(2) $400 \leqslant T_a \leqslant 600\,^{\circ}$C: The substitutional fraction increases at the expense of the interstitial fraction. At 600 °C the interstitial fraction has almost completely converted into a substitutional one. The fact that the total $S_{Ga} + T_{As}$ fraction remains constant indicates that Mn_I converts into Mn_{Ga} by combining with Ga vacancies (V_{Ga}) created during implantation. We will discuss this mechanism below in terms of the thermal stability and diffusion of Mn_I.

(3) $T_a > 600\,^{\circ}$C: While the interstitial fraction remains negligible, the substitutional fraction decreases from nearly 100% at 600 °C to nearly 50% at 700 °C, in both the n^+ and semi-insulating samples (not measured for p^+ GaAs[12]). We will discuss this below in terms of diffusion of substitutional Mn.

1. Interstitial Mn

In the low doping regime investigated here, the thermal stability of interstitial Mn is not affected by the presence of acceptor (Zn_{Ga}) or donor (Te_{As}) defects. This independence requires that two basic mechanisms through which the doping type generally affects the diffusivity of charged defects in semiconductors were inefficient in this particular case: (i) change in free-carrier density (which affects the charge screening of charged defects) and (ii) change in charge state and concentration of trapping defects. Free-carrier density is likely not to play a role in the materials studied here, since the deep centers introduced during implantation are likely to shift the Fermi level towards the middle of the band gap. Discussing the lack of observable trapping of interstitial Mn requires a closer look at the concentrations of the potential trapping acceptor and donor defects. The order of magnitude of the dopant (Zn and Te) concentrations can be estimated from the quoted carrier concentration (before implantation) assuming a 100% activation. After implantation, the Mn_{Ga} (Mn_I) fraction contributes to the corresponding acceptor (donor) concentration as well. Note that, although the Mn implantation is likely to shift the Fermi level towards the middle of the band gap, the concentration of *charged* donors (Te_{As} and Mn_I) and acceptors (Zn_{Ga} and Mn_{Ga}) is in principle unaffected, because shallow donors and acceptors remain positively and negatively charged, respectively, when the Fermi level moves deeper into the band gap. The concentration of potential trapping defects, i.e., charged donors (Te_{As} and Mn_I) and acceptors (Zn_{Ga} and Mn_{Ga}), are compiled in Table II, as well as the corresponding mean donor-donor and acceptor-acceptor distances. Since varying the concentration of potential trapping defects by an order of magnitude (and thus varying the mean distance between them and the Mn_I defects by a factor of almost 3) produced no measurable change in the thermal stability of Mn_I, these can be ignored in the following modeling of the Mn_I migration.

As mentioned above, the fact that the total $S_{Ga} + T_{As}$ fraction remains constant indicates that Mn_I converts into Mn_{Ga} by combining with Ga vacancies (V_{Ga}) created during implantation. However, estimating the migration barrier of Mn_I, i.e., the activation energy (E_a) for free interstitial diffusion, requires that the concentration profiles of both Mn_I and V_{Ga} (before each of the annealing steps) are known. Nevertheless, using the model which we applied to the p^+ case,[12] it is possible to obtain estimates for the maximum and minimum E_a values as follows. Within an Arrhenius model for the thermally activated migration, the fraction $f(T, \Delta t)$ of

TABLE II. Estimated acceptor (Zn_{Ga} and Mn_{Ga}) and donor (Te_{As} and Mn_I) concentrations and mean donor-donor and acceptor-acceptor distances. The dopant (Zn and Te) concentrations were estimated from the quoted carrier concentration assuming a 100% activation. The Mn_{Ga} and Mn_I peak concentrations were estimated from the ^{56}Mn peak concentration (x_p in Table I) and the S_{Ga} and T_{As} fractions measured for the annealing temperatures 100–300 °C (i.e., $x_p \times$ fraction). The mean acceptor-acceptor and donor-donor distances are estimated from the total acceptor (Zn_{Ga} and Mn_{Ga}) and donor (Te_{As} and Mn_I) concentrations, respectively, assuming a random distribution of all four defects. The values corresponding to our previous work on p^+ GaAs[12] are also included.

Doping type	Dopant	Acceptor concentration (cm^{-3})	Donor concentration (cm^{-3})	Mn_{Ga} (acceptor) peak concentration (cm^{-3})	Mn_I (donor) peak concentration (cm^{-3})	Mean acceptor-acceptor distance (Å)	Mean donor-donor distance (Å)
n^+	Te	–	$1.1 - 5 \times 10^{18}$	3.2×10^{18}	1.6×10^{18}	85	65
s.i.	–	–	–	4.7×10^{18}	2.0×10^{18}	79	54
p^+	Zn	$1.4 - 6 \times 10^{19}$	–	3.8×10^{18}	1.4×10^{18}	34	90

Mn remaining on T_{As} sites after an annealing step of duration Δt at a temperature T is given by

$$f(T,\Delta t) = f_0 \exp[-\nu_0 \Delta t / N \exp(-E_a/k_B T)], \quad (1)$$

where f_0 is the T_{As} fraction before the annealing step; ν_0 is the attempt frequency, which we take as 10^{12} s^{-1}, i.e., of the order of the lattice vibrations; k_B is the Boltzmann constant; and N is the average number of jumps before a Mn_I atom combines with a Ga vacancy.[28] There are two unknown parameters in Eq. (1), E_a and N. Therefore, in order to estimate E_a from our data, it is necessary to fix N. Although N cannot be determined independently, it is possible to deduce the minimum and maximum N values, and consequently the maximum and minimum values of E_a consistent with our data, taking two extreme and opposite scenarios before the mobilization of Mn_I: (i) every Mn_I (in T_{As}) has trapped one mobile V_{Ga} in a neighboring Ga tetrahedron and (ii) Mn_I and V_{Ga} are randomly and independently distributed. Case (i) requires a minimum N of one jump of the Mn atom from T_{As} into the Ga vacancy. Case (ii) corresponds to a maximum N of 20 000, based on conservative assumptions regarding the annealing dynamics of V_{Ga} (described in Ref. 12). With N between 1 and 20 000, Eq. (1) yields an activation energy of 1.7–2.3 eV, similar to p^+ GaAs.[12]

The main conclusion from the above analysis is that the high activation energy for Mn_I diffusion in GaAs (1.7–2.3 eV), determined here and in Ref. 12, cannot be ascribed to acceptor trapping, since varying the acceptor concentration by an order of magnitude has no measurable effect. Such high activation energy for diffusion should thus be a characteristic of isolated interstitial Mn. This does not mean that trapping of Mn_I impurities by acceptor defects does not happen in general. In the low concentration regime studied here, it is very likely that trapping does not occur simply because Mn_I defects combine with Ga vacancies before being trapped by substitutional acceptors. Indeed, MARLOWE[29] simulations of the distribution of the implanted ^{56}Mn impurities and of the Ga vacancies created upon implantation yield a mean distance between a Mn impurity and the nearest Ga vacancy of the order of 2 Å, i.e., much smaller than the distance between Mn impurities and the nearest substitutional acceptors. Even though in practice the mean Mn_I-V_{Ga} distance is larger than 2 Å due to vacancy annealing, these estimates are a good indicator that, indeed, Mn_I impurities combine with Ga vacancies before being trapped by substitutional acceptors, thus explaining the equal diffusion behavior for the different doping types.

2. Substitutional Mn

The decrease in the substitutional Mn fraction from nearly 100% at 600 °C to nearly 50% at 700 °C indicates Mn diffusion, either (i) long-range diffusion to the sample bulk or surface, without clustering, or (ii) within the implanted layer, with clustering.

In a scenario where substitutional Mn diffuses to the sample bulk or surface [scenario (i)], electrons emitted from deeper within the sample (diffusion to the bulk) are subject to stronger dechanneling, whereas electrons emitted from the first few atomic layers (diffusion to the surface) do not experience channeling effects and thus contribute with an isotropic ("random") pattern. Both effects result in a decreased fitted fraction. Diffusion of substitutional Mn in GaAs can be modeled by a Frank-Turnbull mechanism: a Mn atom "jumps" from the substitutional site and diffuses through interstitial sites until being trapped by a Ga vacancy (V_{Ga}), thus becoming substitutional (Mn_{Ga}) again. The next "diffusion step" occurs when the atom leaves the vacancy and is trapped by another one. Assuming the V_{Ga} concentration is fixed, such a process follows an Arrhenius behavior. The corresponding activation energy is given by the binding energy of the Mn impurity to V_{Ga} plus the migration energy of interstitial Mn diffusion. The Mn_{Ga} fraction measured after an annealing step of duration Δt at a temperature T is thus given by Eq. (1), where N is in this case the number of steps until the ^{56}Mn emitter is either too deep to contribute with a measurable channeling effect or at the surface. Assuming that the concentration of Ga vacancies that survived annealing up to 700 °C is very low, only one diffusion step is required, i.e., $N = 1$. As such, Eq. (1) yields $E_a = 2.9$ eV (c.f. Fig. 4), which is in agreement with a recent radio-tracer study on the diffusion of Mn in GaAs,[30] yielding an activation energy of ∼3 eV.

In a clustering scenario [scenario (ii)], substitutional Mn precipitates into a phase which is not perfectly coherent with the cubic GaAs lattice (e.g., disordered cubic $Ga_xMn_{1-x}As$,[31] hexagonal $Ga_xMn_{1-x}As$,[32] or hexagonal MnAs[31]), thus decreasing the substitutional fraction. However, detecting such precipitates in samples with such a small number of Mn impurities as in our case (2×10^{13} cm^{-2}) is extremely challenging, and beyond the scope of this work, focused on the diffusion of interstitial Mn. Nevertheless, diffusion of substitutional Mn leading to precipitation can roughly be modeled with Eq. (1) assuming, as in scenario (i), that the concentration of Ga vacancies that survived annealing up to 700 °C is very low, i.e., only one diffusion step ($N = 1$) is required for diffusing Mn to be trapped in precipitates. The estimated activation energy is therefore the same as for the scenario of long-range diffusion without precipitation ($E_a = 2.9$ eV), and consistent with the radio-tracer measurements mentioned above.[30]

3. Comparison to higher Mn concentrations

As summarized above, our main conclusion is that the high activation energy for diffusion E_a (1.7–2.3 eV), in the low doping regime investigated here (<0.05% Mn), does not result from trapping by neighboring charged defects, but is an intrinsic characteristic of isolated interstitial Mn. The fact that the reported activation energy in highly Mn-doped GaAs (few percent Mn) is at least 1 eV lower (0.7 eV)[10] may be related to its metallic character. In highly doped metallic $Ga_{1-x}Mn_xAs$, charge screening of interstitial Mn by the free carriers may decrease the migration barrier compared to the low Mn doping regime. It is important to note, however, that increasing Mn concentration increases the probability of formation of Mn_{Ga}-Mn_I pairs. In fact, at a few percent Mn, all interstitial Mn is likely to be in a Mn_{Ga}-Mn_I pair configuration, as can be deduced from the efficient magnetic self-compensation due to antiferromagnetic coupling between the substitutional and the interstitial Mn moments in a pair.[7] As mentioned above, the binding energy of such pairs has been estimated to increase by up to 0.8 eV the effective activation energy for diffusion of

interstitial Mn.[13] This, in turn, implies that the mechanism responsible for decreasing the migration barrier of *isolated* Mn_I with increasing Mn concentration would have to be remarkably efficient, in order to overcome the effect of pair formation which is on the opposite direction. Such complex interplay of screening and trapping effects, as well as the fact that previous experimental work (although extensive) is in many cases indirect (lacking element or site specificity, for example), motivate a detailed assessment of the thermal stability and diffusion of interstitial Mn in $Ga_{1-x}Mn_xAs$, from the very dilute to the high Mn concentration regime. Experimentally, this requires a method which unambiguously identifies interstitial Mn and quantitatively tracks its fraction as a function of annealing temperature or time: for example, β^- emission channeling experiments, similar to the ones presented here, but on $Ga_{1-x}Mn_xAs$ thin films grown by low-temperature molecular-beam epitaxy. Such experiments should also take into account the effect of annealing atmosphere, as it is currently understood that capless annealing in vacuum is less efficient for inducing Mn out-diffusion, compared to annealing in air[7] or in vacuum but with an amorphous arsenic capping layer.[33,34]

IV. CONCLUSIONS

We have experimentally determined the lattice location of Mn impurities (<0.05%) in undoped (semi-insulating) and heavily *n*-type doped GaAs, as a function of annealing temperature up to ∼700 °C. In addition to the majority substituting for Ga, a significant fraction occupies tetrahedral interstitial sites with As nearest neighbors. Similar to our recent report on heavily *p*-type doped GaAs, the interstitial fraction is stable up to 400 °C, with an activation energy for diffusion of 1.7–2.3 eV. Substitutional Mn becomes mobile at higher temperatures (∼700 °C) with an activation energy of ∼3 eV.

Since the concentration of potential trapping defects has no measurable effect on the activation energy for diffusion of the interstitial fraction (as far as the recombination with nearby Ga vacancies is concerned), we conclude that the observed high thermal stability is characteristic of isolated interstitial Mn in GaAs. Compared to the high doping regime (few percent Mn), where a significantly lower activation energy has been reported, these findings challenge the current understanding of how the interplay between the free-carrier concentration and the concentration of trapping centers affects the diffusion of interstitial Mn in Mn-doped GaAs.

ACKNOWLEDGMENTS

This work was supported by the Portuguese Foundation for Science and Technology (CERN/FP/116320/2010,SFRH/BD/35761/2007, PTDC/FIS/66262/2006), the European Union Seventh Framework through ENSAR (European Nuclear Science and Applications Research, Contract No. 262010) and SPIRIT (Support of Public and Industrial Research Using Ion Beam Technology, Contract No. 227012), the Fund for Scientific Research—Flanders, KU Leuven Project No. GOA/2009/006, and the IUAP (Interuniversity Attraction Poles) P6/42 program.

*lino.pereira@fys.kuleuven.be

[1] T. Dietl, H. Ohno, F. Matsukura, J. Cibert, and D. Ferrand, Science **287**, 1019 (2000).
[2] K. Sato, P. H. Dederics, and H. Katayama-Yoshida, Europhys. Lett. **61**, 403 (2003).
[3] K. Alberi, K. M. Yu, P. R. Stone, O. D. Dubon, W. Walukiewicz, T. Wojtowicz, X. Liu, and J. K. Furdyna, Phys. Rev. B **78**, 075201 (2008).
[4] M. Dobrowolska, K. Tivakornsasithorn, X. Liu, J. K. Furdyna, M. Berciu, K. M. Yu, and W. Walukiewicz, Nat. Mater. **11**, 444 (2012).
[5] T. Dietl, D. D. Awschalom, M. Kaminska, and H. Ohno, *Spintronics* (Academic, New York, 2008), Vol. 82.
[6] T. Dietl, Nat. Mater. **9**, 965 (2010).
[7] T. Jungwirth *et al.*, Phys. Rev. B **72**, 165204 (2005).
[8] S. Mack, R. C. Myers, J. T. Heron, A. C. Gossard, and D. D. Awschaloma, Appl. Phys. Lett. **92**, 192502 (2008).
[9] T. Hayashi, Y. Hashimoto, S. Katsumoto, and Y. Iye, Appl. Phys. Lett. **78**, 1691 (2001).
[10] K. W. Edmonds *et al.*, Phys. Rev. Lett. **92**, 037201 (2004).
[11] K. M. Yu, W. Walukiewicz, T. Wojtowicz, I. Kuryliszyn, X. Liu, Y. Sasaki, and J. K. Furdyna, Phys. Rev. B **65**, 201303 (2002).
[12] L. M. C. Pereira, U. Wahl, S. Decoster, J. G. Correia, M. R. da Silva, A. Vantomme, and J. P. Araújo, Appl. Phys. Lett. **98**, 201905 (2011).
[13] V. I. Baykov, P. A. Korzhavyi, and B. Johansson, Phys. Rev. Lett. **101**, 177204 (2008).
[14] B. L. Sheu, R. C. Myers, J. M. Tang, N. Samarth, D. D. Awschalom, P. Schiffer, and M. E. Flatte, Phys. Rev. Lett. **99**, 227205 (2007).
[15] H. Hofsäss and G. Lindner, Phys. Rep. **201**, 121 (1991).
[16] U. Wahl *et al.*, Nucl. Instrum. Methods Phys. Res. A **524**, 245 (2004).
[17] U. Wahl, J. G. Correia, S. Cardoso, J. G. Marques, A. Vantomme, G. Langouche, and ISOLDE Collaboration, Nucl. Instrum. Methods Phys. Res. B **136**, 744 (1998).
[18] S. Agostinelli *et al.*, Nucl. Instrum. Methods Phys. Res. A **506**, 250 (2003).
[19] J. Allison *et al.*, IEEE Trans. Nucl. Sci. **53**, 270 (2006).
[20] H. Hofsäss, U. Wahl, and S. G. Jahn, Hyperfine Interact. **84**, 27 (1994).
[21] H. Hofsäss, Hyperfine Interact. **97**, 247 (1996).
[22] U. Wahl, Hyperfine Interact. **129**, 349 (2000).
[23] U. Wahl, J. G. Correia, J. P. Araújo, E. Rita, and S. J. C, Appl. Phys. Lett. **90**, 181934 (2007).
[24] L. M. C. Pereira, U. Wahl, S. Decoster, J. G. Correia, L. M. Amorim, M. R. da Silva, J. P. Araújo, and A. Vantomme, Phys. Rev. B **84**, 125204 (2011).
[25] J. F. Ziegler, J. P. Biersack, and M. D. Ziegler, *The Stopping and Range of Ions in Matter* (Lulu Press, Maryland, USA, 2009).

[26]V. N. Fedoseyev *et al*., Nucl. Instrum. Methods Phys. Res. B **126**, 88 (1997).
[27]U. Wahl, A. Vantomme, G. Langouche, and ISOLDE Collaboration, Nucl. Instrum. Methods Phys. Res. B **148**, 492 (1999).
[28]U. Wahl, J. G. Correia, E. Rita, J. P. Araújo, and J. C. Soares (ISOLDE Collaboration), Nucl. Instrum. Methods Phys. Res. B **253**, 167 (2006).
[29]M. T. Robinson, Phys. Rev. B **40**, 10717 (1989).
[30]O. Koskelo, J. Raisanen, F. Tuomisto, and J. Sadowski (ISOLDE Collaboration), Sem. Sci. Tech. **24**, 045011 (2009).
[31]A. Kwiatkowski, D. Wasik, M. Kaminska, R. Bozek, J. Szczytko, A. Twardowski, J. Borysiuk, J. Sadowski, and J. Gosk, J. Appl. Phys. **101**, 113912 (2007).
[32]J. Sadowski, J. Z. Domagala, R. Mathieu, A. Kovacs, T. Kasama, R. E. Dunin-Borkowski, and T. Dietl, Phys. Rev. B **84**, 245306 (2011).
[33]M. Adell, J. Adell, L. Ilver, J. Kanski, J. Sadowski, and J. Z. Domagala, Phys. Rev. B **75**, 054415 (2007).
[34]V. Stanciu, O. Wilhelmsson, U. Bexell, M. Adell, J. Sadowski, J. Kanski, P. Warnicke, and P. Svedlindh, Phys. Rev. B **72**, 125324 (2005).